

## Research Paper

**Cite this article:** Agarwal S, Sharma A, Zuazola IJG, Kumar M (2023). A compact SWB MIMO antenna with 45° clock-wise square patch inclusions for polarization diversity applications. *International Journal of Microwave and Wireless Technologies* **15**, 513–525. <https://doi.org/10.1017/S1759078722000435>

Received: 6 July 2021

Revised: 15 March 2022

Accepted: 17 March 2022

First published online: 11 April 2022

### Key words:


Annular ring antenna; bandwidth dimension ratio; defected ground structure; multiple-input multiple-output; polarization diversity

### Author for correspondence:

Ashwani Sharma,

E-mail: [ashwani.sharma@iitrpr.ac.in](mailto:ashwani.sharma@iitrpr.ac.in)

# A compact SWB MIMO antenna with 45° clock-wise square patch inclusions for polarization diversity applications

Shobit Agarwal<sup>1</sup>, Ashwani Sharma<sup>1</sup> , Ignacio J. Garcia Zuazola<sup>2</sup> and Manoj Kumar<sup>1</sup>

<sup>1</sup>Department of Electrical Engineering, Indian Institute of Technology Ropar, Rupnagar, Punjab, India and <sup>2</sup>School of Computing and Digital Media, London Metropolitan University, 166-220 Holloway Rd, London N7 8DB, UK

## Abstract

In this paper, a compact super wideband annular ring antenna using 45° clock-wise square patch inclusions for super high frequency and polarization diversity applications is proposed. The inclusions consist of a combination of squares and circles into one another in the inner area of a main annular ring radiator. The antenna uses a partial ground plane having a stair-type defected ground structure, is designed on an FR-4 substrate, and has a total size of  $25 \times 26 \times 1.6 \text{ mm}^3$  ( $0.17\lambda \times 0.18\lambda$ ). The design was fabricated and experimental results fairly agreed with simulations and resulted in an antenna with an operating frequency from 2.07 to 30 GHz; that is, a large fractional bandwidth of 174.2% with a bandwidth (BW) ratio of 14.5:1 and a high BW dimension ratio, BW per unit electrical length of 5693, and a measured peak gain of 8 dBi with an average gain of 5 dBi for the overall operating frequency. For the polarization diversity, a  $4 \times 4$  multiple input-multiple output configuration is additionally presented, offering an effective isolation of  $\geq 22.5$  dB between ports and corroborated by measurements.

## Introduction

The increasing demand for communication systems with high spectral performance and high data rates is driving the growth of improved communication devices. Ultra-wideband (UWB) communication and the UWB planar antennas can provide short-range communication using the 3.1–10.6 GHz allocated spectrum; however, wireless personal area network consumers have personal interest in super wideband (SWB) transceivers that cover both short- and long-range communication with wider bandwidth (BW), high data rate, increased coverage, and maximum resolution. An SWB antenna can be customized for the purpose and should ideally be designed for a BW ratio of at least 10:1 for return loss of  $\leq 10$  dB and, based on the propagation demands, be either omnidirectional or directional. In the literature, numerous SWB antennas have been reported.

In [1], a coplanar waveguide (CPW)-fed planar elliptical antenna for SWB applications showed a BW ratio of 21.6:1 and in [2] using a semi-elliptical patch radiator a BW ratio of 19.7:1 is obtained. These designs, however, partially covered the entire UWB frequency spectrum. In [3], the same authors further improved the BW achieved in [1] by introducing a semicircular-shaped branch connected to the tapered feed line of the patch antenna; this led to an impedance BW from 1.02 to 24.1 GHz. A similar design presented in [4] achieved an impedance BW from 1.08 to 27.4 GHz and a compact version of the same design [5] improved the lower frequency range and BW dimension ratio (BDR) performance. In contrast, to achieve wider impedance BW, a tailored patch radiator was used in [6] with a tapered feed line. A similar technique was used in [7] to further enhance the BW ratio to 34:1. SWB performance reported an impedance BW from 0.65 to 35.61 GHz and a BW ratio of 54.78:1. Although the designs from [4–9] provided high impedance BW, BW ratio, and BDR, their relatively large sizes (smallest footprint  $80 \times 80 \text{ mm}^2$  [9]) are not opportunistic for small equipment integration.

An egg-shaped planar monopole antenna with dimensions  $35 \times 77 \text{ mm}^2$  is reported [10] for SWB applications. It uses a semi-elliptical fractal-complementary slot into an asymmetrical ground to achieve an impedance BW of 172%, that is, from 1.44 to 18.8 GHz. In [11], a CPW-fed propeller-shaped SWB planar antenna of size  $38 \times 55 \text{ mm}^2$  is reported. This design offers a super-wide impedance BW from 3 to 35 GHz and a BW ratio of 11.6:1; however, its attained BDR was 805 which is relatively low. In [12], a semi-circular-shaped monopole antenna with a trapezoidal ground plane was investigated where a tapered feed line was used to excite the semi-circle patch. This design of size  $52 \times 42 \text{ mm}^2$  provides a BDR of 4261 for an impedance BW from 1.3–20 GHz and BW ratio of 15.38:1. A smaller profile antenna of size  $30 \times 40 \text{ mm}^2$  was designed in [13] based on a parasitic oval patch built in

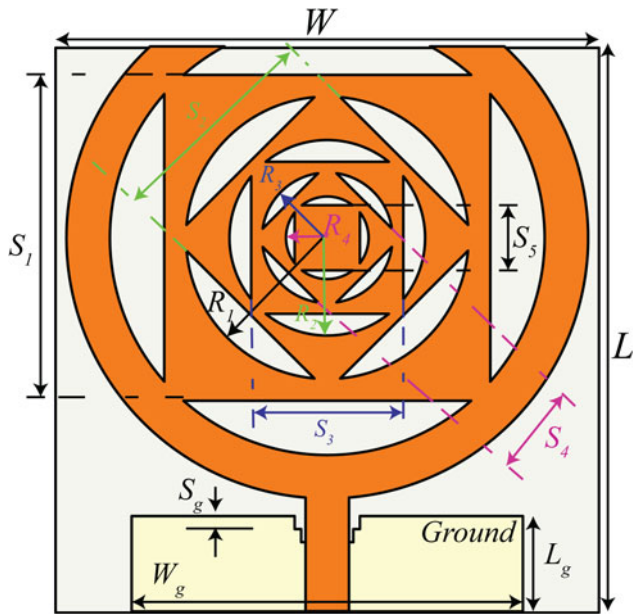


Fig. 1. Geometry of the proposed SWB antenna.

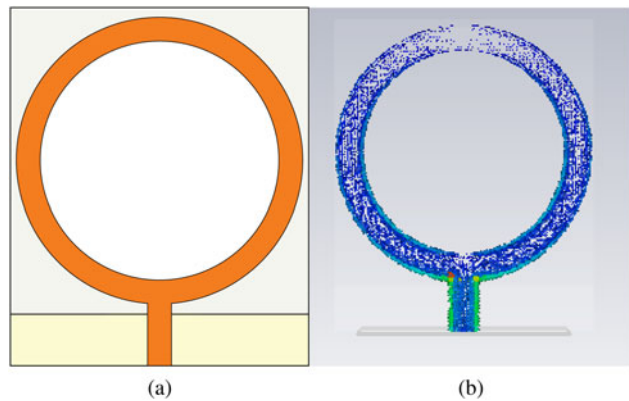


Fig. 2. (a) Conventional annular ring antenna and (b) surface current distribution.

an elliptical slot and a microstrip-line-fed elliptical tuning fork element. This led to an antenna with an impedance BW of 19.92 GHz measured from 2.26 to 22.18 GHz. In [14], a CPW-fed transparent antenna of size  $45 \times 30 \text{ mm}^2$  was presented for enhanced impedance BW. A staircase rectangular radiator was used to generate overlapped resonant frequencies and complemented with two major and minor symmetrical rectangular stubs in the ground plane to increase BW. This led to an impedance BW of 28.85 GHz measured from 3.15 to 32 GHz, however, its BDR of 1127 is still relatively low, though the BW ratio is 10.16:1. The immediately outlined literature review reveals that enhancing the impedance BW of an antenna either compromises its overall size or its BDR performance. Therefore, a compact antenna having an SWB characteristic with high BDR is challenging here.

As stated earlier, because of the rich spectrum resource, high transmission rate, strict secrecy, and low power consumption requirements, SWB systems have received a lot of attention. To improve multipath fading capability, multiple input-multiple output (MIMO) antenna configurations are attractive. With

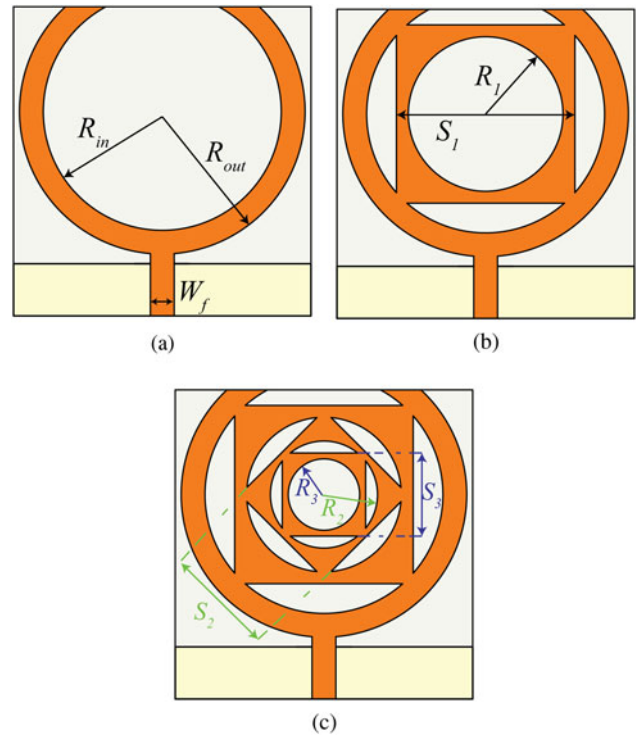


Fig. 3. Evolution of the proposed antenna: (a) evolved 0 design, (b) evolved 1 design, and (c) evolved 2 design.

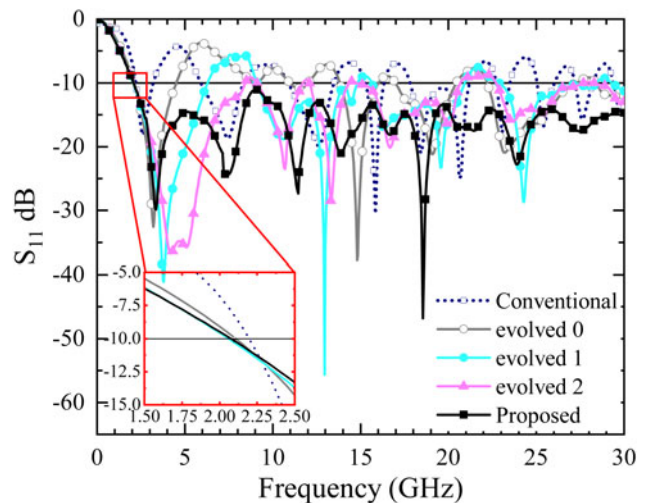
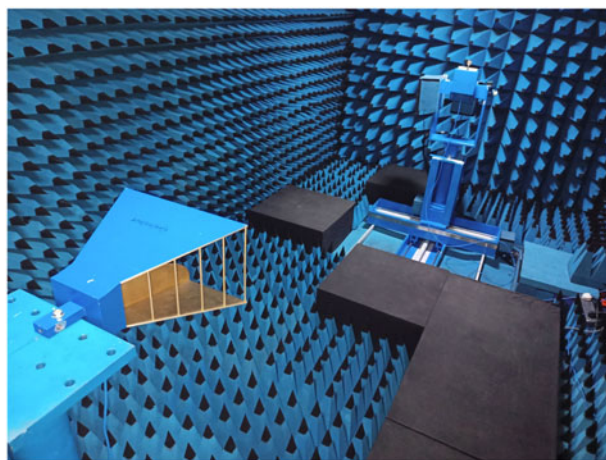


Fig. 4. Simulated  $S_{11}$  parameters of evolved antennas.

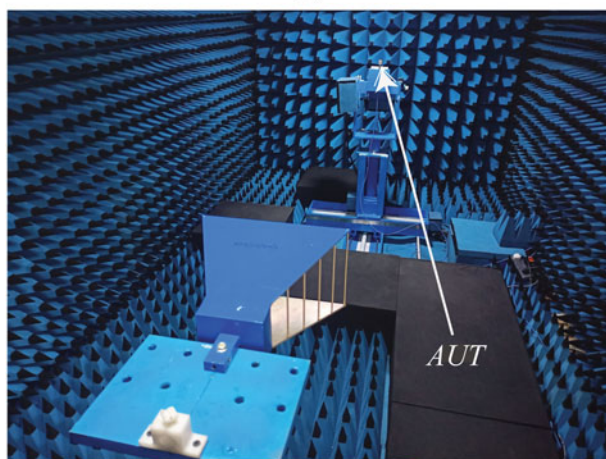
this, the propagation distance can be enhanced for a given input power. The use of MIMO antenna configurations for SWB applications with high isolation among the multiple antenna elements is challenging. In [15] a split-ring resonator arrangement was used to achieve a band-notch, and a T-shaped slot was made in the ground plane to improve isolation between antennas, which was below  $-15 \text{ dB}$  in the operating band. A rectangular slot and T-shaped stub in the ground plane were made for a dual-polarized UWB-MIMO antenna [15], lowering the coupling between antennas to less than  $-20 \text{ dB}$ . Using polarization diversity, a four-element UWB-MIMO antenna has been

**Table 1.** Dimensions of the proposed antenna

Parameter	Value (mm)	Parameter	Value (mm)
$L$	25	$R_2$	4.5
$W$	26	$R_3$	3
$L_g$	4.39	$R_4$	1.9
$W_g$	18	$S_1$	15
$S_g$	0.6	$S_2$	10
$W_f$	2	$S_3$	7
$R_{out}$	12	$S_4$	4.8
$R_{in}$	10	$S_5$	3
$R_1$	6.5	-	-



(a)

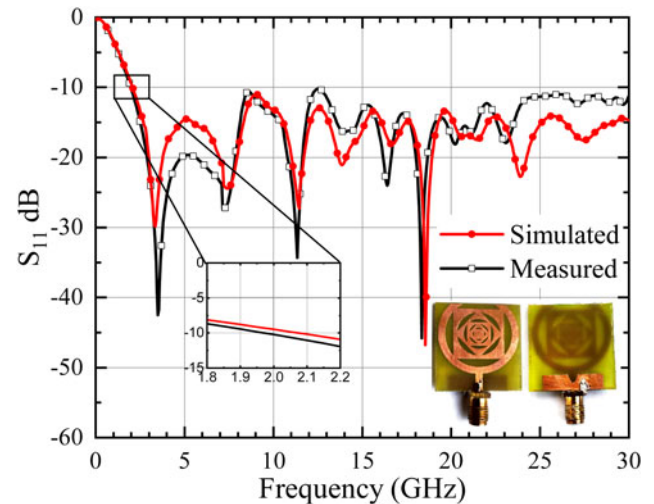


(b)

**Fig. 5.** Measurement setup inside an anechoic chamber.

presented in [16]. An integrated four-element UWB-MIMO antenna based on frequency reconfiguration was fabricated for cognitive radio applications in [17].

In this paper, a compact SWB annular ring antenna using 45° clock-wise square patch inclusions for super high frequency (SHF) and polarization diversity applications is proposed.

**Fig. 6.**  $S_{11}$  parameters of the proposed antenna with the fabricated prototype.

The inclusions consist of square patches with inscribed etched circles and is fed using a 50  $\Omega$  microstrip line. The antenna offers a fractional bandwidth (FBW) of 174.2% over the operating frequency ( $f_0$ ) of 2.97–30 GHz and is suitable for SHF applications including Wi-Fi/WLAN, WiMAX, radar communication, satellite and defense communication, and mm-wave communication. For the polarization diversity a 4  $\times$  4 MIMO configuration is devised and manufactured, offering an effective isolation of  $\geq 22.5$  dB between ports and corroborated by measurements. Following the proposed antenna introduction, its design and evolution, is given in Section “Proposed antenna design and evolution,” its fabrication and validation in Section “Fabrication and validation,” a time-domain analysis using the proposed antenna as a transmitter (Tx) and as a receiver (Rx) in Section “Time-domain analysis,” a MIMO configuration in Section “MIMO configuration,” and concluding remarks are provided in the final section.

### Proposed antenna design and evolution

The geometry of the proposed compact SWB annular ring antenna using 45° clock-wise square patch inclusions for SHF applications is shown in Fig. 1.

The inclusions consist of square patches ( $S_{1-5}$ ) with inscribed etched circles ( $R_{1-4}$ ) and form the radiating elements of the antenna. The design is symmetrical along the vertical axis and it will be shown attractive to allow the current distribution to remain symmetric throughout the design evolution. It uses a partial ground plane with a 4-stair-type defect at the back of the substrate (Fig. 1) for good impedance matching over the BW and etched on a commercially available FR-4 substrate having dielectric constant  $\epsilon_r = 4.4$ , substrate height  $h = 1.6$  mm, and loss tangent  $\tan \delta = 0.02$ . A 50  $\Omega$  microstrip line fed the antenna whose dimensions were calculated using standard equations [18] and iteratively optimized for optimum performance. CST Microwave Studio was used for the design and led to a compact prototype  $W, \sim L$  (Fig. 1) of  $25 \times 26$  mm<sup>2</sup> ( $0.17\lambda \times 0.18\lambda$ ).

Initially, a conventional annular ring antenna, Fig. 2(a), was designed using standard equations [19] and conveniently simulated. Observations on the surface maximum current distribution, shown in Fig. 2(b), suggested the removal of the area in which the currents are low. Most of the currents were concentrated toward

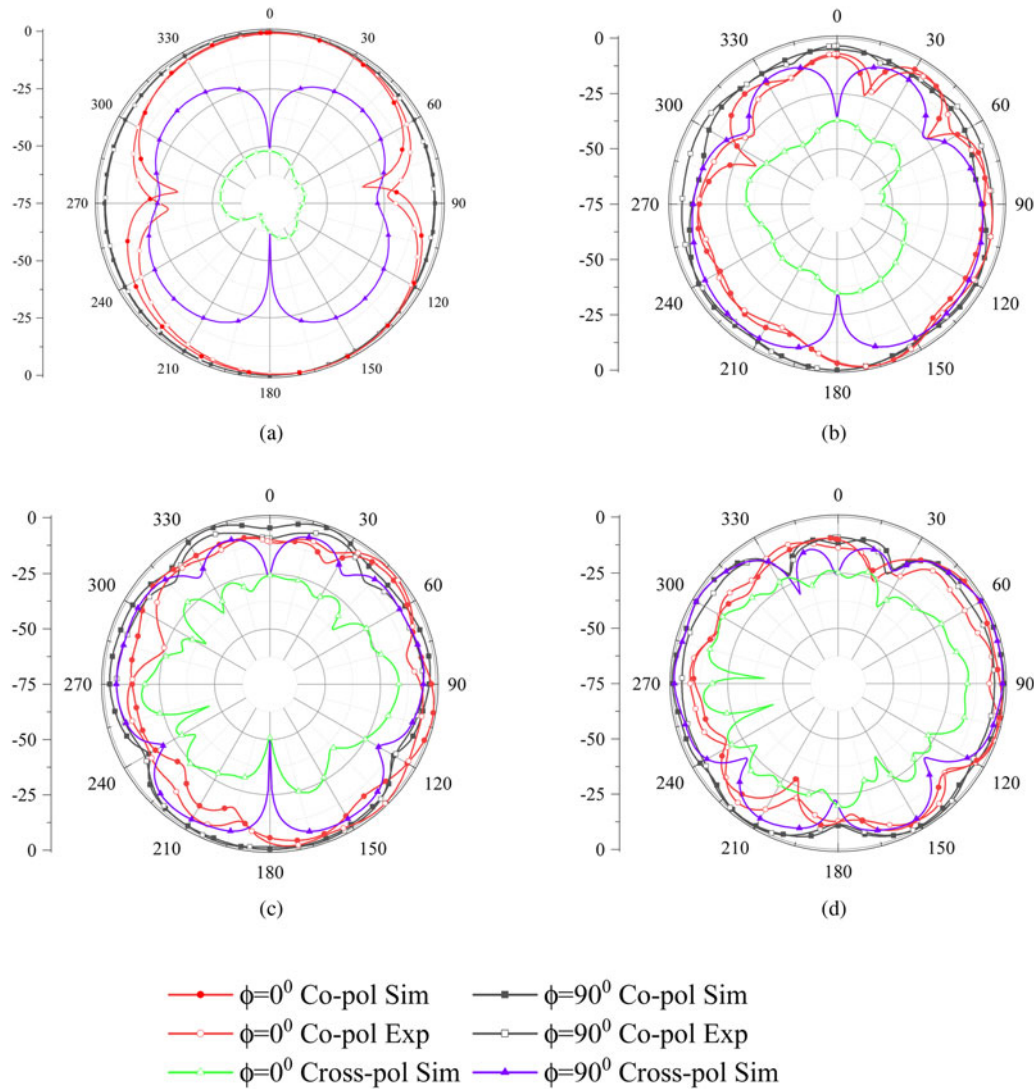


**Fig. 7.** Simulated and measured radiation patterns of the proposed antenna at (a) 5 GHz, (b) 13 GHz, (c) 21 GHz, and (d) 28 GHz.

the feed line with minimal concentrations opposite to the feed. This area of minimal concentrations was removed and resulted in a relatively smaller design; this is presented in Fig. 3(a) and termed as evolved 0 design.

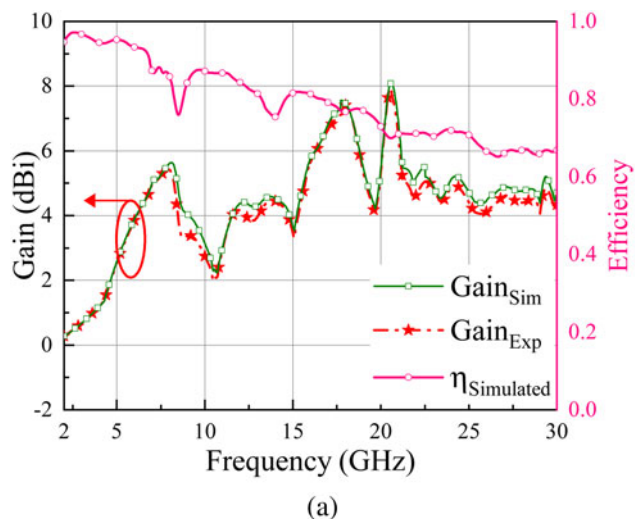
The simulated reflection coefficient ( $S_{11}$ ) of the conventional annular ring antenna and evolved 0 to 2 are shown in Fig. 4. Results show evolved 0 design with  $f_0$  of 2.1–4.5, 10.95–12, 13.83–16, 17–20.45, 22.2–27.25, and 28.4–30 GHz measured at  $-10$  dB and leading to a multi-band antenna.

Next, to achieve a SWB response by maintaining same physical size, a square patch of side  $S_1$  having a circular slot of radius  $R_1$  was included in the inner area of the annular ring of evolved 0 design; the resulting design is shown in Fig. 3(b) referred to it as evolved 1. Adding these structures help in increasing the electrical length of the antenna by providing multiple paths for the current to pass. As a result, the evolved 1 design resonated in the 2.05–6.28, 9.1–14.80, 15.65–20.90, 22.90–28.42, and 29.32–30 GHz frequency bands (measured at  $-10$  dB).

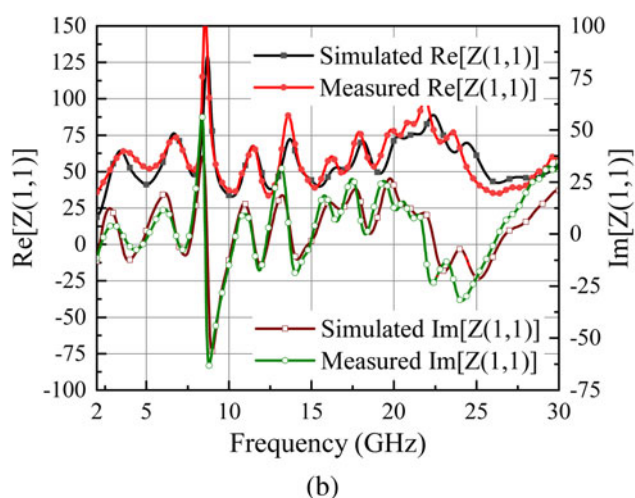
Additional inclusions were performed to further increase the BW performance to form the final evolved design. This was

made by two more clock-wise  $45^\circ$  rotated square patches of sides  $S_2$  and  $S_3$  having circular slots of radii  $R_2$  and  $R_3$  respectively, Fig. 3(c). This led to the evolved 2 design with satisfactory performance over the intended frequency range. However, impedance mismatch was observed (Fig. 4) at 8.5, 11.8, 14.5, and 20.7–22.7 GHz measured at  $-10$  dB.

Finally, referred as proposed design (Fig. 1), two additional square patches of side  $S_4$  and  $S_5$  were included in the previous evolved 2 design out of which the fourth square ( $S_4$ ) is having a circular slot of radius  $R_4$ . This resulted in an impedance matching away from the initially intended  $50 \Omega$  specially at the high frequency ( $f_h$ ) of operation and to accommodate this, a stair-type defect was made in the ground plane. This led to a proposed compact SWB annular ring antenna design using  $45^\circ$  clock-wise square patch inclusions for SHF applications with a  $f_0$  between 2.07 and 30 GHz (measured at  $-10$  dB). From the inset of Fig. 4, it can also be seen that, the lower cut-off frequency shifts mainly for the first inclusion and not others. Since the lowest cut-off frequency is caused by the outermost structures, it does not change much for inner inscribed shapes. On the contrary, the



(a)



(b)

Fig. 8. Simulated and measured (a) gain and efficiency and (b) input impedance of the proposed antenna.

inner shapes improve the response at higher frequencies by generating multiple constructive resonances. This is further validated by Fig. 9.

The final dimensions of the proposed antenna are listed in Table 1.

### Fabrication and validation

The proposed antenna was fabricated and measured. A Power Network Analyzer (PNA-L) N5234B by Agilent Technologies was used for the experiments. Anechoic chamber setup for antenna measurement is shown in Fig. 5.

The fabricated prototype and  $S_{11}$  parameters of the fabricated antenna (compared to simulated) are shown in Fig. 6.

Experimental results show a compact SWB annular ring antenna using  $45^\circ$  clock-wise square patch inclusions for SHF applications having a BW of 28 GHz over the  $f_0$  of 2–30 GHz. Measured and simulated results are in fair agreement as shown in Fig. 6. The simulated (co- and cross-polar) and measured (co-polar) radiation patterns of the antenna are shown in Fig. 7. Only relevant patterns measured at 5, 13, 21, and 28 GHz are shown. The patterns are all pretty much omnidirectional for the

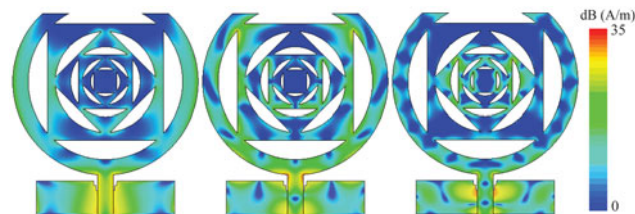


Fig. 9. Simulated maximum current densities of the proposed antenna: (a) 5 GHz, (b) 15 GHz, and (c) 28 GHz.

$H$ -plane ( $\phi = 90^\circ$ ) and dipole-like for the  $E$ -plane ( $\phi = 0^\circ$ ); this is more apparent at 5 GHz, Fig. 7(a). At higher frequencies 13, 21, and 28 GHz, Figs 7(b)–7(d), the  $E$ -plane is not that dipole-like also  $H$ -plane is not omnidirectional due to the excitation of higher order modes [9], however, these modes did not present a negative influence in real applications. Also, the level of cross-polarized patterns is approaching toward co-polar patterns for some angles. This also occurs due to excitation of higher order modes at higher frequencies. Measured and simulated results are in fair agreement, validating the fabricated antenna.

The gain was measured and corroborated with simulations as shown in Fig. 8(a). Peak gains of 8 dBi are recorded for the simulated and measured results with strong agreement between both the results. The gain pattern is in accordance with [14, 20–23]. Figure 8(b) shows the input impedance of the antenna. Although it is normal to vary over the  $f_0$ , fair agreement is seen with simulated results validating the results. The real and imaginary values are seen fluctuating around 50 and  $0 \Omega$  respectively what is perceived as an appropriate input impedance for the proposed SWB antenna.

Furthermore, to gain an insight into antenna performance for entire frequency range, current density at three different frequencies is shown in Fig. 9. It is evident from the figure that at 5 GHz, the current density was denser along the annular ring near the feed line while at higher frequencies, 15 and 28 GHz, uniformly dense over the radiator (annular ring + patch inclusions). That means, as the frequency increased more current densities were observed in the inner inclusions. Because of these inclusions, the current-carrying conductor (the radiator) was lengthier and the current density around the circumference got redistributed.

To corroborate the performance of the proposed SWB antenna is to characterize the percentage BW provided per unit electrical area, the BDR. For SWB antennas, a high BDR is preferred to ensure maximum BW per unit electrical area of the design [1]. Mathematically, the BDR is expressed as,

$$BDR = \frac{\%BW}{\lambda_l \times \lambda_w} \quad (1)$$

where  $\%BW$  is the percentage BW of the antenna,  $\lambda_l$  and  $\lambda_w$  are antenna length and width corresponding to  $f_i$ .

Using this BDR measurement and other comparative measures, a comparison study was carried out with other reported literature prototypes and summarized in Table 2. Results show that the proposed design is miniaturized by 7.67% compared to the smallest prototype and provide comparable gain than reported in the literature. The proposed antenna provides a wider BW compared to [1–7, 9, 10, 12, 13, 21, 23–27] and better BW ratio and  $\%BW$  compared to [10, 11, 13, 14, 21, 24, 25, 27, 28] with a higher BDR compared to all designs except for [24, 25] but

**Table 2.** Comparison study with the literature

Ref.	Size ( $L \times W$ ) (mm <sup>2</sup> )	Size ( $\lambda_l \times \lambda_w$ ) (mm <sup>2</sup> )	$f_0$ (GHz)	BW ratio	%BW	BDR	Peak gain (dBi)	Size (%) compared to the proposed antenna
[1]	140 × 120	0.19 × 0.16	0.4 – 9.51	21.6:1	183.85	5092.8	4	96.13
[2]	140 × 120	0.21 × 0.18	0.46 – 9.07	19.7:1	180.7	5736.5	5	96.13
[3]	124 × 110	0.37 × 0.42	1.02 – 24.1	23.63:1	183.7	1167	7	95.23
[4]	124 × 120	0.43 × 0.44	1.08 – 27.40	25:1	184.8	959	6.2	95.63
[5]	80 × 80	0.186 × 0.186	0.7 – 20	28.57:1	193	3362	7	89.84
[6]	150 × 156	0.21 × 0.20	0.4 – 16	40:1	190.2	4515	6	97.22
[7]	150 × 150	0.36 × 0.36	0.72 – 25	34.72:1	188.8	1457	7	97.11
[8]	170 × 150	0.325 × 0.368	0.65 – 35.61	54.78:1	193	1613.7	6.5	97.45
[9]	80 × 80	0.08 × 0.08	0.3 – 20	66.6:1	194	3233	7	89.84
[10]	35 × 77	0.17 × 0.37	1.44 – 18.8	13.05:1	172	2735	7	75.88
[11]	38 × 55	0.55 × 0.38	3–35	11.66:1	168	805	4	68.90
[12]	52.25 × 42	0.22 × 0.18	1.3–20	15.38:1	175.6	4261	4.18	70.38
[13]	30 × 40	0.30 × 0.23	2.26–22.18	9.81:1	163	2393.7	6.5	45.83
[14]	45 × 30	0.47 × 0.31	3.15–32	10.16:1	164.1	1126.6	– 4.8	51.85
[21]	30 × 35	0.32 × 0.27	2.7–28.8	10.66:1	165.7	1948	5	38.09
[23]	135 × 135	0.45 × 0.45	1–19.4	19.4:1	180.4	890.8	2	96.43
[24]	52 × 42	0.16 × 0.13	0.96–13.98	14.56:1	174.3	7468.5	5.8	70.24
[25]	52 × 46	0.17 × 0.13	0.95–13.80	14.52:1	174.23	7871.5	6	72.83
[26]	62 × 64	0.347 × 0.358	1.68–26	15.48:1	175.72	1414.5	3	83.62
[27]	32 × 22	0.27 × 0.18	2.5–29	11.6:1	168.2	3462	3.65	7.67
[28]	40 × 40	0.345 × 0.345	2.59–31.14	12.02:1	169	1419.9	5	59.38
[29]	130 × 120	0.37 × 0.34	0.86–30	34.88:1	188.8	1473.1	–	95.83
[30]	74 × 80	0.28 × 0.26	1.05–32.7	31.14:1	187.5	2586	–	89.02
[22]	31 × 45	0.22 × 0.32	2.18–44.5	20.41:1	181.3	2467	4.4	53.40
[31]	40 × 30	0.41 × 0.31	3.1– 94.7	30.54:1	187.3	1473	3.48	45.83
Proposed	25 × 26	0.17 × 0.18	2.07–30	14.5:1	174.2	5693	8	–

Here,  $\lambda_l$  and  $\lambda_w$  are normalized length and width (in wavelengths) corresponding to the lowest operating frequency.

these present narrower BW, therefore not overcoming the proposed design.

### Time-domain analysis

To measure the performance of the proposed antenna in time domain, a time-domain analysis was performed as arranged in Figs 10(a) and 10(b) and using two identical proposed antennas as the Tx and Rx. The normalized amplitudes of both input and output pulses for the two different configurations are shown in Fig. 10(c). There are no apparent ringing effects in the input and output signals (Fig. 10(c)) and just output signals decaying over the time. Fidelity factor (FF), which defines the

cross-correlation between transmitted and received signals, is calculated using (2):

$$FF = \max \left[ \frac{\int_{-\infty}^{\infty} S_t(t) S_r(t + \tau) dt}{\int_{-\infty}^{\infty} |S_t(t)|^2 dt \int_{-\infty}^{\infty} |S_r(t)|^2 dt} \right]. \quad (2)$$

where  $S_t(t)$  and  $S_r(t)$  indicate transmitted and received signals and  $\tau$  the group delay. The computed values of FF are listed in Table 3.

Group delay is a measure of the transition time taken by the signal to pass through a device and it signifies the negative rate of transfer function phase with respect to the frequency [32].

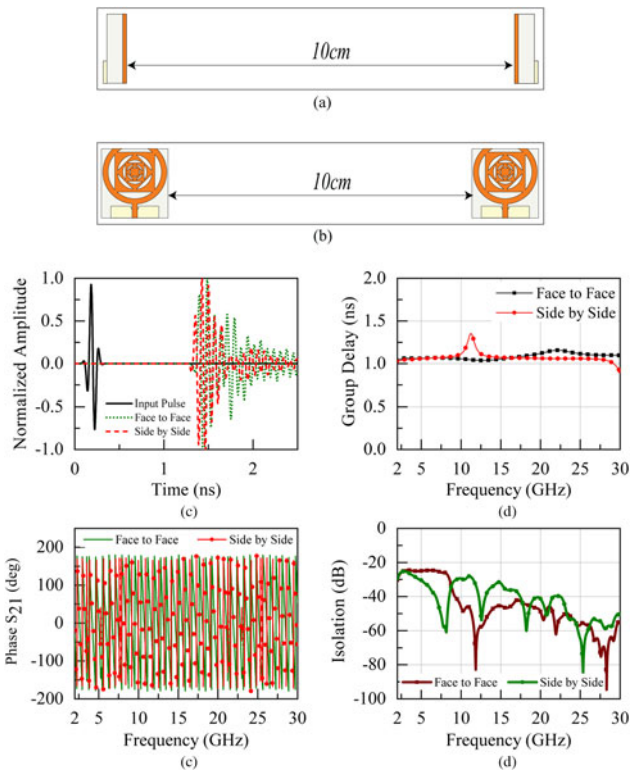


**Fig. 10.** Time-domain analysis of the proposed antenna: (a) face-to-face configuration, (b) side-by-side configuration, (c) input and output signals, (d) group delay, (e) phase, and (f) isolation.

**Table 3.** FF of the proposed antenna

	Face-to-face	Side-by-side
Fidelity factor	92%	85%

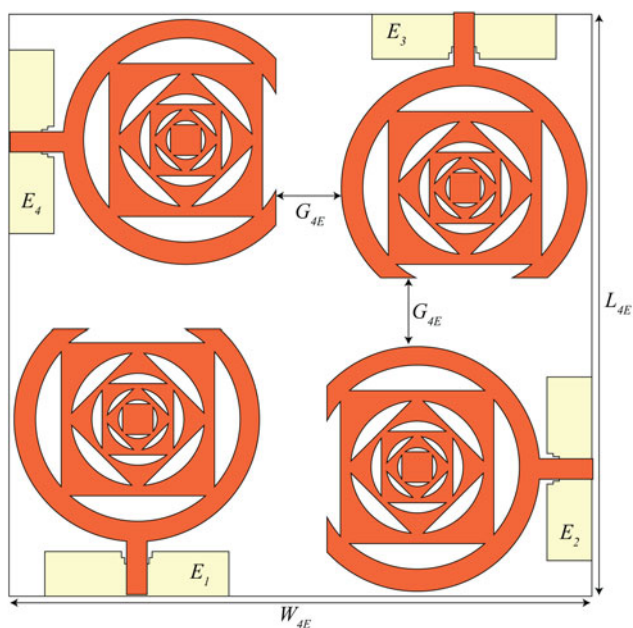


**Fig. 11.** MIMO configuration for polarization diversity:  $L_{4E} = 56$  mm,  $W_{4E} = 56$  mm,  $G_{4E} = 5$  mm.

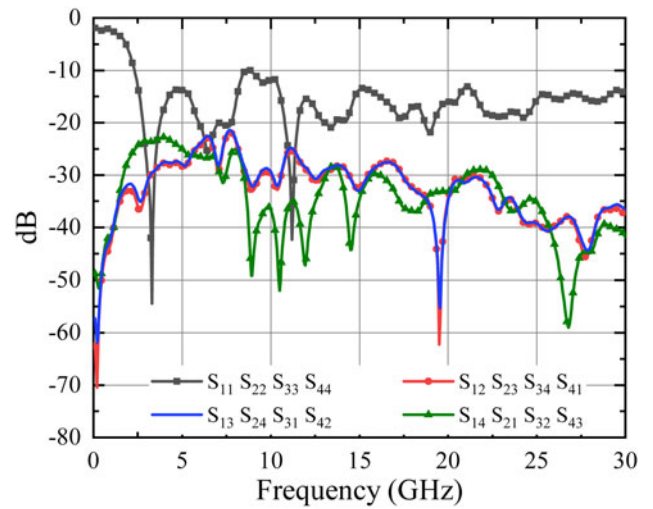
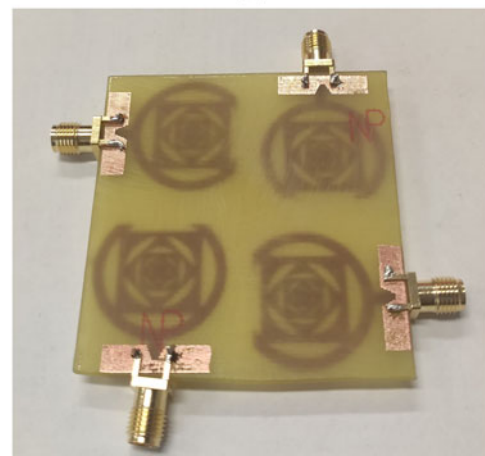


**Fig. 12.** Simulated reflection coefficient and isolation.



(a)



(b)

**Fig. 13.** Fabricated prototype of 4 × 4 MIMO array: (a) front view and (b) back view.

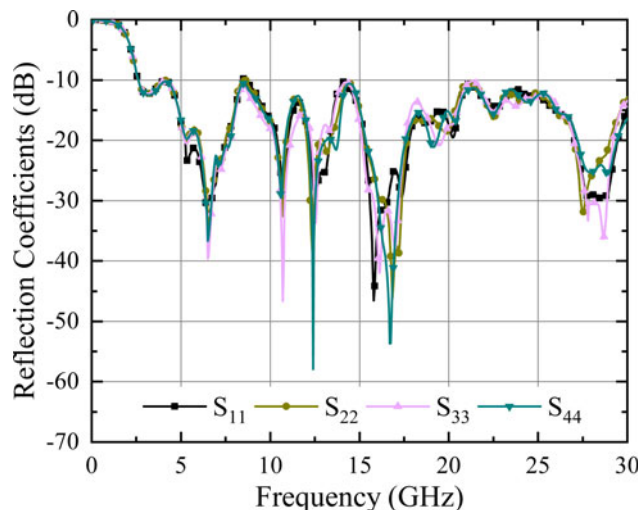


Fig. 14. Measured reflection coefficients of the array.

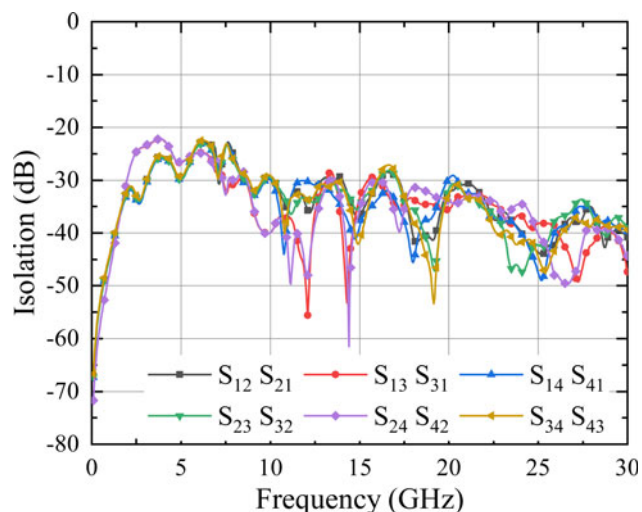


Fig. 15. Measured isolation parameters of the array.

Mathematically, group delay is expressed as

$$\tau_g(\omega) = -\frac{d\phi(\omega)}{d\omega} = -\frac{d\phi(\omega)}{2\pi df} \quad (3)$$

Simulated results of  $\tau_g(\omega)$  for both the configurations are shown in Fig. 10(d). Practically, for SWB antennas group delay should be within 1 ns [33] to ensure the phase linearity in the far-field region and no pulse distortion is present.

Isolation is defined by the ratio of incident power on input port and delivered power at the output port. This also characterizes the coupling between both the ports. A high value of magnitude of isolation,  $|S_{21}|$ , represents an uncorrelated transmission between the ports. The simulated response for both the configurations is shown in Fig. 10(f). It can be observed from the figure that  $S_{21} \leq -25$  dB for the operating range.

Figure 10(e) shows phase variation of  $S_{21}$  with respect to frequency. A linear variation of phase signifies that there is no out of phase component in the received signal within the operating

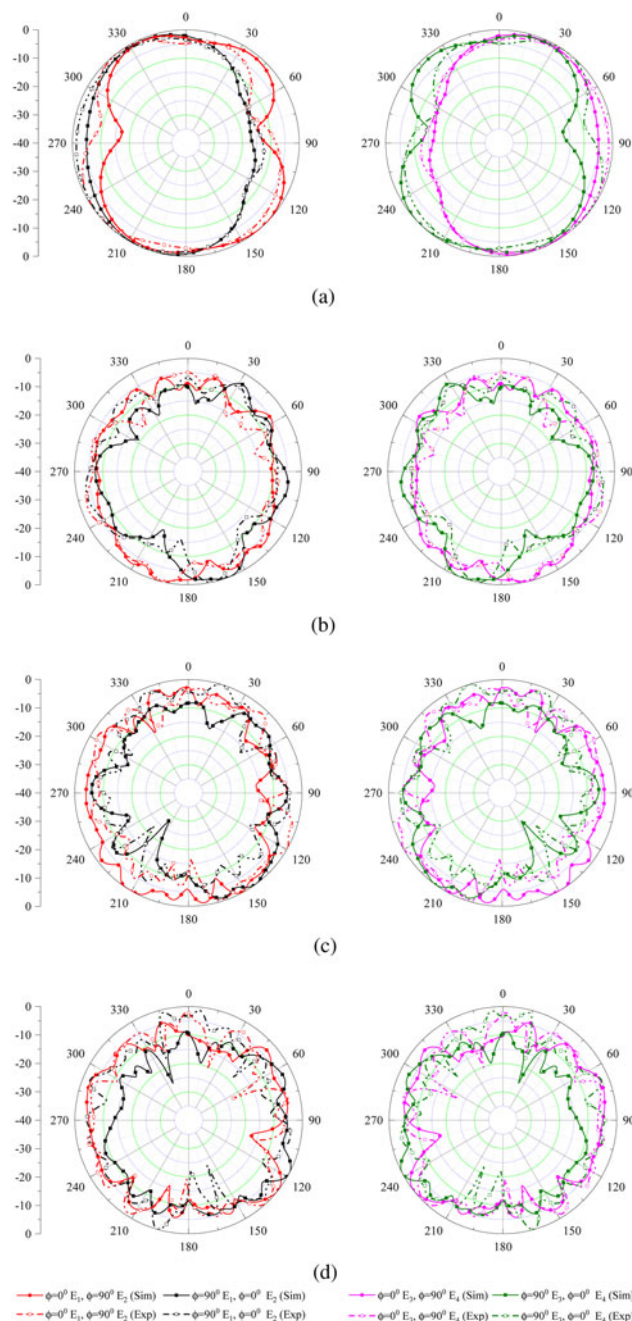


Fig. 16. Simulated and measured radiation patterns of the array at (a) 5 GHz, (b) 13 GHz, (c) 21 GHz, and (d) 28 GHz.

range. For the proposed antenna, a linear variation of the phase is recorded within its operating range.

### MIMO configuration

To exploit polarization diversity, the proposed antenna is arranged in a 4x4 MIMO configuration, next. Four elements,  $E_i \in i = 1, 2, 3, 4$ , are etched on an FR-4 substrate of length  $L_{4E} = 56$  mm, width  $W_{4E} = 56$  mm, and thickness 1.6 mm with a structure shown in Fig. 11.

A polarization shift between adjacent elements that form the array is  $90^\circ$  given the arranged orientation of these elements



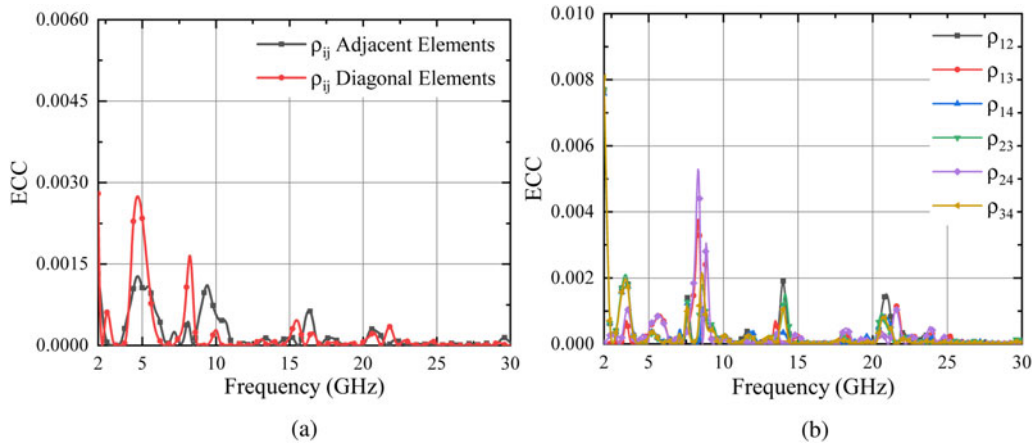


Fig. 17. ECC performance of the array: (a) simulated and (b) measured.

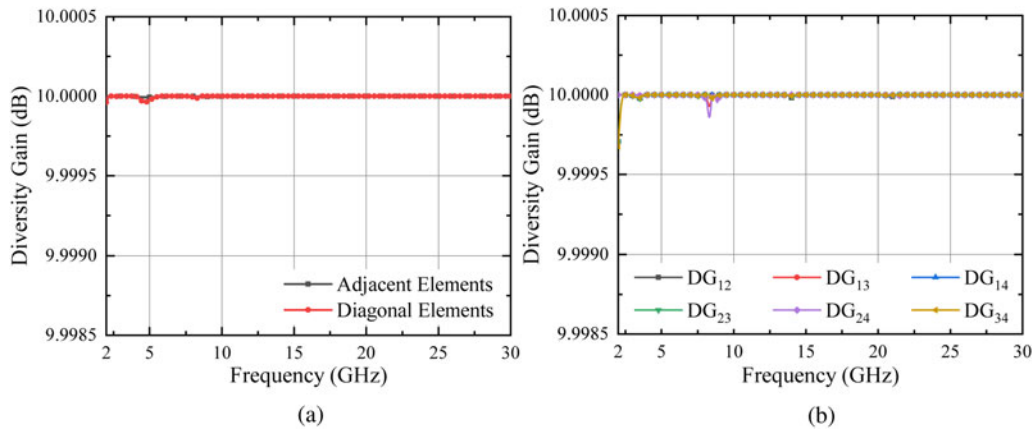


Fig. 18. Diversity gain of the array: (a) simulated and (b) measured.

(Fig. 11). A gap,  $G_{4E}$ , of 5 mm is used between the adjacent elements to accord with the convention that gap  $\geq \lambda/2$  for low mutual coupling.

The simulated reflection coefficient and isolation of the array are given in Fig. 12 and show confirmation of the proposed SWB response (from 2.07 to 30 GHz) with isolation between ports  $\geq 22.5$  dB.

To validate the results, the prototype was fabricated. This is shown in Fig. 13 and the corresponding reflection coefficient and isolation between ports in Figs 15(a) and 15(b), respectively.

Measurements corroborated simulations; the insignificant discrepancies were due to fabrication tolerances. Since the proposed polarization diversity configuration has array elements which are arranged in a quadratic orientation, hence, the radiation characteristics are expected to mimic the same behavior. The  $E$ -plane ( $\phi = 0^\circ$ ) radiation pattern of  $E_1$  is therefore equal to  $H$ -plane ( $\phi = 90^\circ$ ) radiation pattern of  $E_2$  and vice versa. To validate this, the simulated and measured radiation patterns of the array at four distinct frequencies are shown in Figs 16(a)–16(d). It can be observed from the results that simulated and measured results are in good agreement and also satisfy the expected behavior of polarization diversity configuration.

The performance parameters of the array are evaluated next.

### Envelope correlation coefficient and diversity gain

Envelope correlation coefficient (ECC) is one of the key parameters to evaluate the MIMO antenna performance that provides the degree of similarity between received signals. The ECC should ideally be zero and practically as low as possible within the operating frequency ( $f_0$ ) range. The simulated and measured ECC performance of the  $4 \times 4$  array is shown in Figs 17(a) and 17(b), respectively.

In a uniform propagation environment, the ECC is formulated in terms of S-parameters [34] as

$$\rho_{ij} = \frac{|S_{ii}^* S_{ij} + S_{ji}^* S_{jj}|^2}{(1 - (|S_{ii}|^2 + |S_{ji}|^2))(1 - (|S_{jj}|^2 + |S_{ij}|^2))} \quad (4)$$

In general, the  $ECC \leq 0.5$  is acceptable [35] signifying the admissible threshold level of signal distortion. From Fig. 17, it can be noted that simulated value of  $\rho_{ij}$  for adjacent and diagonal elements is  $\leq 0.0015$  and  $\leq 0.003$  respectively. Furthermore, the measured values of  $\rho_{ij}$  are  $\leq 0.002$  and  $\leq 0.005$  for adjacent and diagonal elements within the operating range. This shows that no signal distortion is present for the array (polarization diversity application). Additionally, low value of ECC indicates good

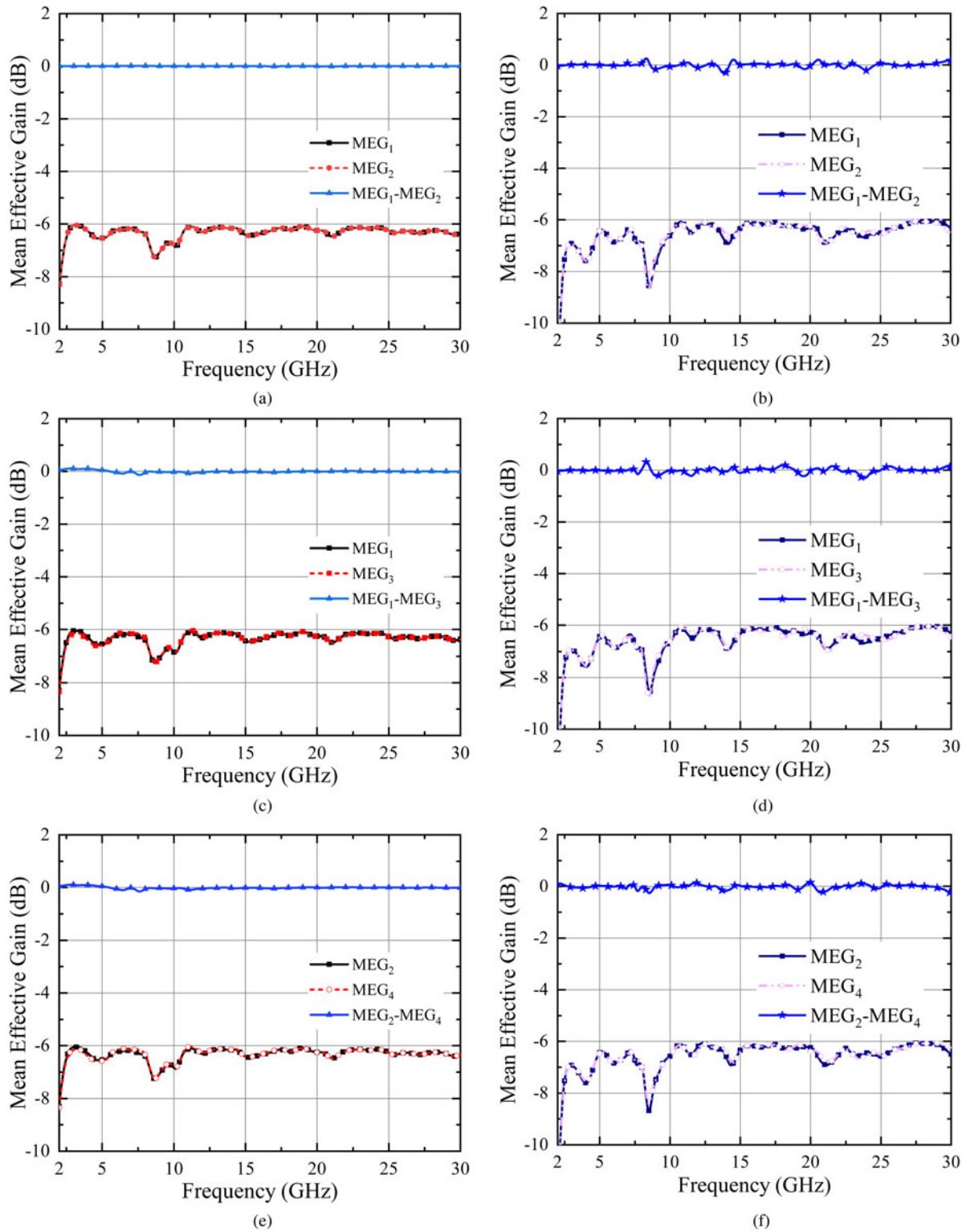


**Fig. 19.** Simulated and measured MEG of the array (a, b) between ports (1, 2), (c, d) between ports (1, 3), and (e, f) between ports (2, 4).

isolation between the array elements, which in turn is helpful for simultaneous operation.

Diversity gain (DG) indicates the improvement obtained from MIMO compared to SISO (single-input single-output) and calculated by the following relation [36]

$$DG \sim (\text{dB}) = 10 \times \log_{10} (10\sqrt{1 - ECC^2}) \quad (5)$$

For satisfactory performance,  $DG \geq 9.95$  dB is desired [37]. The simulated and measured DG of the array is shown in Fig. 18

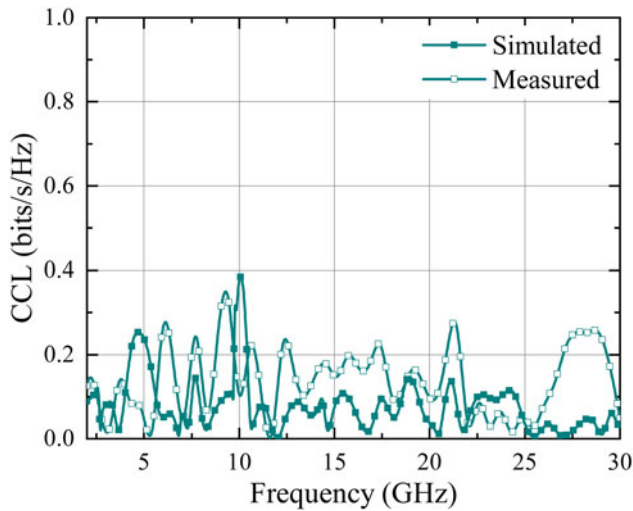


Fig. 20. Simulated and measured CCL of the array.

and is evident that  $DG \approx 10$  dB for both simulation and experimental results within the operating range.

**Mean effective gain**

The mean effective gain (MEG), in practice, is defined as the ratio of power received by MIMO antenna elements to the power received by an isotropic antenna under fading environment. Analytically, the MEG for different element ports can be computed [38] as following with mentioned acceptable limit:

$$MEG_i = 0.5 \left[ 1 - \sum_{j=1}^N |S_{ij}|^2 \right] < -3 \text{ dB} \tag{6}$$

and

$$|MEG_i - MEG_j| \leq 3 \text{ dB} \tag{7}$$

The simulated and measured values of  $MEG_1$  to  $MEG_4$ , and the corresponding differences between different ports are plotted in Figs 19(a)–19(f).

It is concluded from Fig. 19 that the difference between the MEG of two adjacent or diagonal array elements is below the acceptable limit of 3 dB.

**Channel capacity loss**

Channel capacity loss (CCL) denotes the highest transmission rate at which a signal can be continuously transmitted over a communication channel. For faithful transmission, the limit is 0.4 bits/s/Hz within the operating BW [39]. The simulated and measured CCL of the array is shown in Fig. 20.

From the results, it can be concluded that CCL falls within the acceptable limit for the entire operating band.

Table 4 shows a comparison study of the proposed array with the literature. Benefiting from compact SWB antenna elements proposed in this paper, the results show that proposed array is miniaturized by 6.78% compared to the smallest prototype [43] with wider BW and comparable isolation compared to [40–45].

**Conclusion**

A compact SWB annular ring antenna using 45° clock-wise square patch inclusions for SHF and polarization diversity applications is proposed. The antenna provided an SWB operation from 2.07 to 30 GHz with an FBW of 174.2% and a peak gain of 8 dBi and was experimentally validated. For the polarization diversity a 4 × 4 MIMO configuration was devised and manufactured, offering an effective isolation of ≥ 22.5 dB between ports. Its performance in terms of ECC, DG, MEG, and CCL was experimentally validated and found to be well within the specified limit.

Due to its compactness with prominent performance and relatively low cost design, the proposed antenna can be perceived as a suitable candidate for the SHF and polarization diversity applications where SWB is a must.

**Acknowledgement.** This work is supported in part by Department of Science and Technology (DST), Science and Engineering Research Board (SERB), Government of India under grant ECR/2018/000343.

**References**

1. Liang X-L, Zhong S-S and Wang W (2006) Elliptical planar monopole antenna with extremely wide bandwidth. *Electronics Letters*, 42(8), 441–442.

Table 4. Comparison study of the proposed array with the literature

Ref.	Size		No. of ports	$f_0$ (GHz)	%BW	Isolation (dB)	Size (%) compared to the proposed antenna
	mm × mm	$\lambda_l \times \lambda_w$					
[40]	60 × 60	0.60 × 0.60	4	3–16.2	137.5	≥ 17.5	12.89
[41]	100 × 100	1.03 × 1.03	4	3.1–10.6	109.5	≥ 20	68.64
[42]	80 × 80	0.85 × 0.85	4	3.18–11.5	113.3	≥ 15	51
[43]	58 × 58	0.58 × 0.58	4	3–13.5	127.3	≥ 23	6.78
[44]	80 × 80	0.56 × 0.56	4	2.1–20	162	≥ 25	51
[45]	72 × 72	0.67 × 0.67	4	2.8–10.6	116.4	≥ 18	39.50
Proposed	56 × 56	0.38 × 0.38	4	2.07–30	174.2	≥ 22.5	–

Here,  $\lambda_l$  and  $\lambda_w$  are normalized length and width (in wavelengths) corresponding to the lowest operating frequency.

2. Yan X-R, Zhong S-S and Liang X-L (2007) Compact printed semi-elliptical monopole antenna for super-wideband applications. *Microwave and Optical Technology Letters*, **49**(9), 2061–2063.
3. Liu J, Zhong S and Esselle KP (2010) A printed elliptical monopole antenna with modified feeding structure for bandwidth enhancement. *IEEE Transactions on Antennas and Propagation*, **59**(2), 667–670.
4. Liu J, Esselle KP, Hay SG and Zhong S (2011) Achieving ratio bandwidth of 25:1 from a printed antenna using a tapered semi-ring feed. *IEEE Antennas and Wireless Propagation Letters*, **10**, 1333–1336.
5. Rafique U, Ahmed MM, Hassan MM and Khalil H, A modified super-wideband planar elliptical monopole antenna, in *2018 Progress in Electromagnetics Research Symposium (PIERS-Toyama)*, 2018, pp. 2344–2349.
6. Dong Y, Hong W, Liu L, Zhang Y and Kuai Z (2009) Performance analysis of a printed super-wideband antenna. *Microwave and Optical Technology Letters*, **51**(4), 949–956.
7. Liu J, Esselle KP, Hay SG and Zhong S-S (2012) Study of an extremely wideband monopole antenna with triple band-notched characteristics. *Progress in Electromagnetics Research*, **123**, 143–158.
8. Singhal S and Singh AK (2020) Elliptical monopole based super wide-band fractal antenna. *Microwave and Optical Technology Letters*, **62**(3), 1324–1328.
9. Rafique U and Din SU (2018) Beveled-shaped super-wideband planar antenna. *Turkish Journal of Electrical Engineering and Computer Science*, **26**(5), 2417–2425.
10. Chen K-R, Row J-S, et al. (2011) A compact monopole antenna for super wideband applications. *IEEE Antennas and Wireless Propagation Letters*, **10**, 488–491.
11. Gorai A, Karmakar A, Pal M and Ghatak R (2013) A CPW-fed propeller shaped monopole antenna with super wideband characteristics. *Progress In Electromagnetics Research*, **45**, 125–135.
12. Samsuzzaman M and Islam MT (2015) A semicircular shaped super wideband patch antenna with high bandwidth dimension ratio. *Microwave and Optical Technology Letters*, **57**(2), 445–452.
13. Tang M-C, Ziolkowski RW and Xiao S (2014) Compact hyper-band printed slot antenna with stable radiation properties. *IEEE Transactions on Antennas and Propagation*, **62**(6), 2962–2969.
14. Hakimi S, Rahim SKA, Abedian M, Noghabaei S and Khalily M (2014) CPW-fed transparent antenna for extended ultrawideband applications. *IEEE Antennas and Wireless Propagation Letters*, **13**, 1251–1254.
15. Mao CX and Chu QX (2014) Compact coradiator UWB-MIMO antenna with dual polarization. *IEEE Transactions on Antennas and Propagation*, **62**(9), 4474–4480.
16. Khan M, Capobianco A, Asif S, Iftikhar A, Ijaz B and Braaten B (2015) Compact 4 × 4 UWB-MIMO antenna with WLAN band rejected operation. *Electronics Letters*, **51**(14), 1048–1050.
17. Hussain R, Khan MU and Sharawi MS (2019) Design and analysis of a miniaturized meandered slot-line-based quad-band frequency agile MIMO antenna. *IEEE Transactions on Antennas and Propagation*, **68** (3), 2410–2415.
18. Balanis CA (2016) *Antenna theory: analysis and design*. John Wiley & Sons.
19. Kumar G and Ray KP (2003) *Broadband microstrip antennas*. Artech House.
20. Rahman SU, Cao Q, Ullah H and Khalil H (2019) Compact design of trapezoid shape monopole antenna for SWB application. *Microwave and Optical Technology Letters*, **61**(8), 1931–1937.
21. Srifi MN, El Mrabet O, Falcone F, Ayza MS and Essaaidi M (2009) A novel compact printed circular antenna for very ultrawideband applications. *Microwave and Optical Technology Letters*, **51**(4), 1130–1133.
22. Dorostkar MA, Islam MT and Azim R (2013) Design of a novel super wide band circular-hexagonal fractal antenna. *Progress in Electromagnetics Research*, **139**, 229–245.
23. Yeo J and Lee J-I (2014) Coupled-sectorial-loop antenna with circular sectors for super wideband applications. *Microwave and Optical Technology Letters*, **56**(7), 1683–1689.
24. Okas P, Sharma A and Gangwar RK (2017) Circular base loaded modified rectangular monopole radiator for super wideband application. *Microwave and Optical Technology Letters*, **59**(10), 2421–2428.
25. Okas P, Sharma A and Gangwar RK (2018) Super-wideband CPW fed modified square monopole antenna with stabilized radiation characteristics. *Microwave and Optical Technology Letters*, **60**(3), 568–575.
26. Á. Figueroa-Torres C, Medina-Monroy JL, Lobato-Morales H, Chávez-Pérez RA and Calvillo-Téllez A (2017) A novel fractal antenna based on the Sierpinski structure for super wide-band applications. *Microwave and Optical Technology Letters*, **59**(5), 1148–1153.
27. Rahman M, Islam M, Mahmud M and Samsuzzaman M (2017) Compact microstrip patch antenna proclaiming super wideband characteristics. *Microwave and Optical Technology Letters*, **59**(10), 2563–2570.
28. Okan T (2020) A compact octagonal-ring monopole antenna for super wideband applications. *Microwave and Optical Technology Letters*, **62**(3), 1237–1244.
29. Liu J, Esselle KP, Hay SG, Sun Z and Zhong S (2013) A compact super-wideband antenna pair with polarization diversity. *IEEE Antennas and Wireless Propagation Letters*, **12**, 1472–1475.
30. Liu J, Esselle K, Hay S and Zhong S (2013) Compact super-wideband asymmetric monopole antenna with dual-branch feed for bandwidth enhancement. *Electronics Letters*, **49**(8), 515–516.
31. Manohar M, Nemani UK, Kshetrimayum RS and Gogoi AK, A novel super wideband notched printed trapezoidal monopole antenna with triangular tapered feedline, in *2014 International Conference on Signal Processing and Communications (SPCOM)*, 2014, pp. 1–6.
32. Wiesbeck W, Adamiuk G and Sturm C (2009) Basic properties and design principles of UWB antennas. *Proceedings of the IEEE*, **97**(2), 372–385.
33. Cho YJ, Kim KH, Choi DH, Lee SS and Park S-O (2006) A miniature UWB planar monopole antenna with 5-GHz band-rejection filter and the time-domain characteristics. *IEEE Transactions on Antennas and Propagation*, **54**(5), 1453–1460.
34. Blanch S, Romeu J and Corbella I (2003) Exact representation of antenna system diversity performance from input parameter description. *Electronics Letters*, **39**(9), 705–707.
35. Koohestani M, Moreira AA and Skrivervik AK (2014) A novel compact CPW-fed polarization diversity ultrawideband antenna. *IEEE Antennas and Wireless Propagation Letters*, **13**, 563–566.
36. Chandel R, Gautam AK and Rambabu K (2018) Tapered fed compact UWB MIMO-diversity antenna with dual band-notched characteristics. *IEEE Transactions on Antennas and Propagation*, **66**(4), 1677–1684.
37. Rafique U, Agarwal S, Nauman N, Khalil H and Ullah K (2021) Inset-fed planar antenna array for dual-band 5G MIMO applications. *Progress in Electromagnetics Research C*, **112**, 83–98.
38. Kumar A, Ansari AQ, Kanaujia BK and Kishor J (2018) High isolation compact four-port MIMO antenna loaded with CSRR for multiband applications. *Frequenz*, **72**(9–10), 415–427.
39. Choukiker YK, Sharma SK and Behera SK (2013) Hybrid fractal shape planar monopole antenna covering multiband wireless communications with MIMO implementation for handheld mobile devices. *IEEE Transactions on Antennas and Propagation*, **62**(3), 1483–1488.
40. Wu W, Yuan B and Wu A (2018) A quad-element UWB-MIMO antenna with band-notch and reduced mutual coupling based on EBG structures. *International Journal of Antennas and Propagation*, **2018**,
41. Shehata M, Said MS and Mostafa H (2018) Dual notched band quad-element MIMO antenna with multitone interference suppression for IR-UWB wireless applications. *IEEE Transactions on Antennas and Propagation*, **66**(11), 5737–5746.
42. Hasan MN, Chu S and Bashir S (2019) A DGS monopole antenna loaded with U-shape stub for UWB MIMO applications. *Microwave and Optical Technology Letters*, **61**(9), 2141–2149.
43. Raheja DK, Kanaujia BK and Kumar S (2019) Compact four-port MIMO antenna on slotted-edge substrate with dual-band rejection characteristics. *International Journal of RF and Microwave Computer-Aided Engineering*, **29**(7), e21756.

44. **Rekha VSD, Pardhasaradhi P, Madhav BTP and Devi YU** (2020) Dual band notched orthogonal 4-element MIMO antenna with isolation for UWB applications. *IEEE Access*, **8**, 145 871–145 880.
45. **Kumar S, Lee GH, Kim DH, Mohyuddin W, Choi HC and Kim KW** (2020) Multiple-input-multiple-output/diversity antenna with dual band-notched characteristics for ultra-wideband applications. *Microwave and Optical Technology Letters*, **62**(1), 336–345.



**Shobit Agarwal** received his Bachelor's degree in Electronics & Communication Engineering from Rajasthan Technical University (RTU), Kota, India in 2012 and his Master's in Electronics & Communication Engineering degree in 2016 from The LNM Institute of Information Technology, Jaipur, India. He served as one of the core members of the setup committee of the Antenna and Microwave Research Laboratory (AMR) at IIT

Ropar with a vision of fabrication and testing capabilities of all the RF circuits and antennas operating up to 40 GHz and extendable to 110 GHz in future. His research area includes UWB and SWB antennas, MIMO systems, metamaterials, intelligent reflective surfaces, and frequency selective surfaces. He has authored number of research articles in reputed international journals and conferences. He is a graduate student member of the Institution of Electrical and Electronics Engineering (IEEE), USA; IEEE-Antennas and Propagation Society (IEEE-APS), USA.



**Ashwani Sharma** received his Ph.D. in Antenna Engineering from the University of Deusto, Bilbao, Spain in 2015. He received a Master's degree in RF and Communication Systems from ETSIT, Technical University of Madrid (UPM), Spain in 2013, a B.Tech. degree in Communication and Computer Engineering from The LNM Institute of Information Technology, Jaipur, India in 2010. He is currently working as an Assistant professor

at the Indian Institute of Technology Ropar, India, since July 2018. He was a visiting training fellow at the University of Kent, Canterbury, UK during May–August 2014, and a junior research fellow at the Indian Institute of Technology, New Delhi, India during 2010–2011. His research works have been published in various international journals and conferences such as *IEEE Transactions and Letters*, IET journals, and Wiley letters. His current research interests include exploiting field forming techniques in antenna design for wireless power transmission, IoT, and 5G.



**Ignacio Julio Garcia Zuazola** completed his Ph.D. in Electronics (Antennas) part-time program in 2008; viva in 2010, University of Kent, Canterbury, UK, an eMBA in Business (part-time program) in 2016, Cardiff Metropolitan University, UK, a BENG in Telecommunications Engineering in 2003, Queen Mary – University of London, a HND in telecommunications engineering in 2000, North West London – University of Middlesex

and an FPII in industrial electronics in 1995, School of Chemistry & Electronics of Indautxu, Spain. He has academic experience and been employed as Research Associate (2004) at University of Kent, Research Engineer, Grade 9/9 (2006) at University of Wales, Swansea, UK, Research Associate (2008) at University of Kent, Senior Research Fellow (2011) at University of Deusto, Bilbao, Spain, Visiting Senior Research Fellow (2011) at University of Leeds, UK, Research Associate (2014) at Loughborough University, UK, Representative of Spain (2015) at London School of Commerce, UK, and Lecturer in Electronic Engineering (2018) at University of Portsmouth, UK. He holds educational awards in electricity, pneumatic & hydraulics, and robotics and possesses relevant industrial experience, been hired for Babcock & Wilcox (1993), Iberdrola (1995), Telefonica (1997), Thyssen Elevators (1998), Cell Communications (2000), Nokia Bell Labs (2020), and Bilbao Ekintza – Bilbao City Council (2021). He engaged in an SME in electrical wiring (1996), and is currently a Senior Lecturer (2022) at London Metropolitan University (London Met), UK. He has included in Marquis Who's Who in the World 2010 edition and has published in international journals: *IEEE Transactions, IET Proceedings and Electronics Letters*. His current research interests include business development on one hand and single-band and multiband miniature antennas, and the use of electromagnetic-band gap (EBG) structures and frequency-selective surfaces (FSS). He led the antennas research line and supervised and mentored graduate and postgraduate students and currently bids for grants and contributes to the teaching, scientific, technological, and business development of London Met by promoting and increasing branding, research, and innovation. He is an MIET and an SMIEEE.



**Manoj Kumar** received his B.Tech. degree from Punjab Technical University, Kapurthala, India, in 2016, and his Master's degree in Electronics and Communication Engineering from Kurukshetra University, Kurukshetra, India in 2018. He is currently working toward his Ph.D. degree with the Electrical Engineering Department, Indian Institute of Technology, Ropar, Rupnagar, India. His current research

interests include RFID sensors, rectenna design, and base station antenna design.